CDF Note 10355

Search for Anomalous Production of Photon + Jets + Missing Transverse Energy Events in $p\bar{p}$ collisions at $\sqrt{s} = 1.96$ TeV

The CDF Collaboration
(http://www-cdf.fnal.gov)

December 21, 2010

Abstract

Many new physics models predict mechanisms that could produce a γ + jets signature. We search for discrepancies in the γ + jets and γ + jets + missing transverse energy channels, independent of any model, for new physics using 4.8 fb^{-1} of CDF Run II data collected at the Fermilab Tevatron from $p\bar{p}$ collisions at $\sqrt{s} = 1.96$ TeV. We measure a variety of kinematic distributions in the data including the transverse energy of the photon, the transverse energy of the leading jet(s), the invariant mass of the photon + leading jet(s), the invariant mass of the two leading jets, and the total transverse energy in the event. The shapes of these distributions are examined for deviations from expectations based on the Standard Model and non-collision backgrounds. We find that the data in the γ + jets and γ + jets + missing transverse energy channels are consistent with Standard Model predictions.

1 Introduction

We present the findings of a model-independent, signature-based search for anomalous photon (γ) + jets events from $p\bar{p}$ collisions at $\sqrt{s} = 1.96$ TeV using 4.8 fb^{-1} of data recorded by the upgraded Collider Detector at Fermilab (CDF II) [1]. In $\gamma + \geq$1 jet events and $\gamma + \geq$2 jet events, we measure a variety of kinematic distributions including the transverse energy (E_T) of the photon, the transverse energy of the leading jet(s), the invariant mass of the photon + leading jet(s), the invariant mass of the two leading jets, and the total transverse energy in the event (H_T). The shapes of these distributions are examined for deviations from expectations based on Standard Model (SM) processes and other backgrounds.

The Feynman diagrams in Fig. 1(a) and 1(b) illustrate examples of processes that yield the γ + 2 jets signature. It is interesting to search for a discrepancy in a variety of kinematic distributions because a resonance or excess could hint at the existence of a new heavy particle decaying into γ + jets, or a new physics mechanism such as gauge-mediated SUSY breaking (GMSB) [2] or Technicolor [3]. Of particular interest are events with large missing E_T ($\not\!\!E_T$), since many new physics models predict the existence of particles that would evade detection and produce an imbalance of transverse energy; for example, a $\tilde{G}$ from $\tilde{\chi}_1^0 \to \gamma\tilde{G}$. Standard Model γ + jets processes have no intrinsic $\not\!\!E_T$.

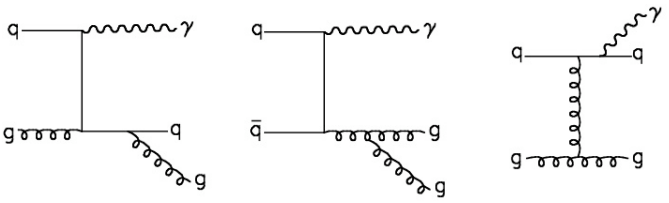

(a)

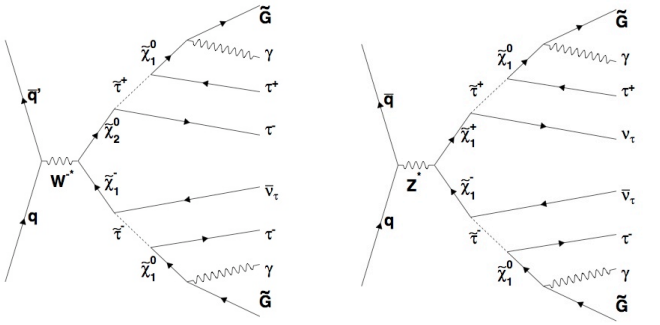

(b)

Figure 1: Feynman diagrams for tree-level (a) Standard Model and (b) GMSB processes that yield the γ + 2 jets signature. The Standard Model processes have no intrinsic $\not\!\!E_T$. A SUSY-like signal may be observed in γ + jets events with large $\not\!\!E_T$.

We present two different methods of determining the backgrounds. In the first method (Method A), we rely on a leading-order Monte Carlo generator (PYTHIA) to predict the kinematic properties of jets in SM γ + jets events. In the second method (Method B), we employ a novel weighting technique that uses a combination of data and Monte Carlo to model higher-order QCD effects in kinematic distributions involving jets.

2 Data Sample and Event Selection

We select a sample of γ candidates by identifying isolated electromagnetic (EM) clusters with $E_T > 30$ GeV in the central region of the calorimeter ($|\eta^{detector}| < 1.1$). In addition, we require the EM cluster to pass standard photon selection requirements [4]. To reduce the background from charged leptons, we require an absence of tracks pointing in the direction of the EM cluster. The background from cosmic rays is reduced with a requirement on calorimeter EM timing [5], and we remove events that originate from the beam halo using a set of topological selection requirements [6]. Events with photomultiplier tube spikes — an instrumentation effect that can resemble a γ — are also removed. In the remaining event sample, we identify one or more jets with $E_T > 15$ GeV and $|\eta^{detector}| < 3.0$. Jet energies are corrected for detector response, energy loss, multiple $p\bar{p}$ interactions and the underlying event [7]. Furthermore, an azimuthal separation of $\Delta\phi > 0.4$ radians between the direction of $\not\!\!E_T$ and any jet above $E_T > 15$ GeV is used to improve the energy measurement of jets.

After applying the event selection requirements described above, we select two data samples based on the number of jets with $E_T > 15$ GeV: $\gamma + \geq$1 jet events and $\gamma + \geq$2 jet events. Within these two samples, subsamples with $\not\!\!E_T > 20$ GeV are identified. By selecting events with large $\not\!\!E_T$, the dominant SM γ and jet backgrounds are reduced, hence increasing our sensitivity to new physics. Various kinematic distributions in each of the four data samples are compared to the background expectation.

3 Modeling Backgrounds

In this analysis we model backgrounds from two main sources: SM processes and non-collision processes. The SM processes include (1) prompt γ production, (2) prompt diphoton production, (3) electroweak production of charged leptons that fake a prompt photon, and (4) QCD production of hadronic jets that fake a prompt photon. The non-collision processes include energetic particles from cosmic rays and the beam halo that mimic the signal of a prompt proton from a $p\bar{p}$ collision. The PYTHIA Monte Carlo generator (Tune A) [8] is used to model SM prompt γ production, prompt diphoton production, and the electroweak charged lepton backgrounds. All other backgrounds are modeled using data. For each of these SM backgrounds and the non-collision background, we construct a background template for each of the kinematic distributions under investigation. The sum of these background templates is then compared to data.

SM diphotons are a significant source of fake $\not\!\!E_T$ background, as the probability to lose one of the photons in an uninstrumented region of the detector is twice as large as in a photon + jet event. The electroweak background is mainly from W, Z, WW, WZ, and ZZ production, in which a final state lepton radiates a photon and we identify it as the prompt photon.

The background from QCD multijet production, in which a jet fakes a photon, is modeled using a sample that consists of jets that pass looser photon selection requirements ("sideband" events). These jets are from neutral mesons like π^0 and η which decay almost exclusively to several photons. This energetic photons cannot be resolved well and are reconstructed as a single isolated photon.

Although a large portion of non-collision backgrounds from cosmic rays and the beam halo is removed by the γ + jets selection requirements, some events remain, and these backgrounds are significant in the large $\not\!\!E_T$ subsamples. A pure cosmic ray event sample is attained using calorimeter EM timing information and is used to construct the background template. A set of topological cuts is used to select beam halo events.

We employ two different methods to construct templates from these background sources. In both methods, the SM diphoton and SM charged lepton background templates are normalized to the expected number of events in the γ + jets data using their respective Monte Carlo production cross sections and the integrated luminosity of the data. The cosmic ray and beam halo templates are normalized to the expected number of background events in the γ + jets data. The two methods differ in their treatment of the SM γ background and the QCD multijet background, as described below.

Method A: We model the SM prompt γ production using the PYTHIA Monte Carlo generator and the QCD multijet background from sideband events. In Method A, these two background templates are scaled so that the total number of SM γ events ($N^{\mathrm{SM}\gamma}$) and the total number of QCD multijet events (N^{QCD}) satisfy

$$N^{\mathrm{QCD}} = f \cdot (N^{\mathrm{SM}\gamma} + N^{\mathrm{QCD}}), \tag{1}$$

where f is the fake photon fraction, which is determined to be

$$f \;=\; 0.319 \pm 0.001(\mathrm{stat}) \pm 0.0068(\mathrm{syst}) \tag{2}$$

from a study of inclusive photon data with photon $E_T > 30$ GeV [4]. In addition, the overall normalization of the SM γ and QCD templates is adjusted so that the total number of background events from all sources equals the number of observed events in the data:

$$N^{\mathrm{Data}} = N^{\mathrm{SM}\gamma} + N^{\mathrm{QCD}} + \underbrace{N^{\mathrm{Di-}\gamma}}_{fixed} + \underbrace{N^{\mathrm{EWK}}}_{fixed} + \underbrace{N^{\mathrm{Non-collision}}}_{fixed}. \tag{3}$$

When used together, Eqs. 1 and 3 uniquely determine $N^{\mathrm{SM}\gamma}$ and N^{QCD}. We note that since the total number of events in the templates is constrained to match the total number of events in the data, our kinematic distributions are not sensitive to anomalies in the overall number of γ + jets events, but they are sensitive to anomalies in the shapes of the distributions and excesses in the tails.

Tables 1 summarizes the Method A background estimates for the $\gamma + \geq 1$ jet and $\gamma + \geq 2$ jet samples. Table 2 summarizes the Method A background estimates for the $\gamma + \geq 1$ jet + $\not\!\!E_T > 20$ GeV and $\gamma + \geq 2$ jet + $\not\!\!E_T > 20$ GeV samples.

Background	**$\gamma + \geq$1 Jet Sample**	**$\gamma + \geq$2 Jet Sample**
Prompt γ	3387044 ± 1840 ± 108938	629569 ± 793 ± 39721
QCD	1472467 ± 1213 ± 27108	273681 ± 523 ± 6095
Electroweak	11765 ± 108 ± 952	1833 ± 42 ± 271
Diphoton	12136 ± 110 ± 641	1775 ± 42 ± 196
Non-Collision	132 ± 11 ± 4	8 ± 2 ± 1
γ + jets Data	4883544 ± 2209	906866 ± 952

Table 1: Summary of background estimates for the $\gamma + \geq 1$ jet and $\gamma + \geq 2$ jet data samples evaluated by Method A. Where two uncertainties are quoted, the first is statistical and the second is systematic.

Background	**$\gamma + \geq$1 Jet + $\not\!\!E_T > 20$ GeV Sample**	**$\gamma + \geq$2 Jet + $\not\!\!E_T > 20$ GeV Sample**
Prompt γ	88878 ± 366 ± 3178	28502 ± 168 ± 1429
QCD	38527 ± 196 ± 1664	12385 ± 111 ± 524
Electroweak	6271 ± 79 ± 613	843 ± 29 ± 122
Diphoton	355 ± 19 ± 13	86 ± 9 ± 8
Non-Collision	124 ± 12 ± 4	8 ± 3 ± 1
γ + jets Data	134155 ± 366	41824 ± 204

Table 2: Summary of background estimates for the $\gamma + \geq 1$ jet + $\not\!\!E_T > 20$ GeV and $\gamma + \geq 2$ jet + $\not\!\!E_T > 20$ GeV data samples evaluated by Method A. Where two uncertainties are quoted, the first is statistical and the second is systematic.

In Method A, the background contributions from SM γ events and QCD multijet events are expected to reproduce many of the kinematic distributions quite well; for example, photon E_T and various invariant masses. Nonetheless, the PYTHIA Monte Carlo event generator used to generate the MC data samples includes only leading-order Feynman diagrams, and this limitation may be apparent in distributions like H_T that rely on the accurate modeling of subleading jets.

Method B: In an attempt to overcome the limitations of using a leading-order Monte Carlo generator to model jet properties in γ + jets events, we implement a novel method in which the QCD multijet events from the sideband data are used as a substitute for the PYTHIA SM γ events. Although the QCD multijet events originate from a different physical process than prompt γ + jets events, we hypothesize that

these events, which come from actual data, describe the properties of jets in γ + jets events better than leading-order Monte Carlo. This should be readily apparent in distributions such as H_T and the number of jets in the event.

Since the sideband data presumably do not contain actual prompt photons, and are only QCD background, we do not expect the reconstructed "QCD photons" in those events to have the same E_T distribution as the actual prompt photons from PYTHIA. We therefore weight the events in the QCD background template in such a way that the weighted QCD template matches the sum of the PYTHIA SM γ and QCD templates for the photon E_T distribution. For an event in bin i of the photon E_T distribution, the associated weight is

$$w_i = \frac{N_i^{SM\gamma} + N_i^{QCD}}{N_i^{QCD}} \tag{4}$$

where $N_i^{SM\gamma}$ and N_i^{QCD} are the contents of each bin i of the background templates determined using Method A. Using Eq. 4, a unique weight can be assigned to every event in the QCD background sample based on the bin i of the QCD photon E_T.

By defining a weight in this manner for every QCD background event, the QCD background template can be weighted for every kinematic distribution. In all of the kinematic distributions, the weighted QCD template replaces the standard QCD template and the SM γ template. In the case of photon E_T, by definition, the weighted QCD background template will be identical to the sum of the SM γ and QCD templates.

This weighting procedure is referred to as Method B. The weighted QCD template is normalized so that the total number of events, $N^{\mathrm{Weighted-QCD}}$, satisfies:

$$N^{\mathrm{Data}} = N^{\mathrm{Weighted-QCD}} + \underbrace{N^{\mathrm{Di-}\gamma}}_{fixed} + \underbrace{N^{\mathrm{EWK}}}_{fixed} + \underbrace{N^{\mathrm{Non-collision}}}_{fixed}. \tag{5}$$

As in Method A, we force the total number of background events to be equal to the total number of data events in each data sample studied. We have calculated an additional systematic uncertainty for weighting procedure, and it is included in the plots of Method B distributions.

Tables 3 summarizes the Method B background estimates for the γ + $\geq$1 jet and γ + $\geq$2 jet samples. Table 4 summarizes the Method B background estimates for the γ + $\geq$1 jet + $\not\!\!E_T > 20$ GeV and γ + $\geq$2 jet + $\not\!\!E_T > 20$ GeV samples.

4 Results

We present results in the γ + jets data with and without the $\not\!\!E_T > 20$ GeV requirement. In the γ + $\geq$1 jet and γ + $\geq$2 jet event samples, we measure the E_T of the photon, the E_T of the leading jet, H_T (scalar sum of all EM objects, jets and $\not\!\!E_T$), $\not\!\!E_T$, and invariant mass of photon and leading jet. In addition, in the γ + $\geq$2 jet sample, we measure the invariant mass of the photon + two leading jets and the invariant mass of the two leading jets.

Background	**γ + $\geq$1 Jet Sample**	**γ + $\geq$2 Jet Sample**
QCD (weighted)	4859511 $\pm$ 2204 $\pm$ 149665	903250 $\pm$ 950 $\pm$ 44525
Electroweak	11765 $\pm$ 108 $\pm$ 952	1833 $\pm$ 42 $\pm$ 271
Diphoton	12136 $\pm$ 110 $\pm$ 641	1775 $\pm$ 42 $\pm$ 196
Non-Collision	132 $\pm$ 11 $\pm$ 4	8 $\pm$ 2 $\pm$ 1
γ + jets Data	4883544 $\pm$ 2209	906866 $\pm$ 952

Table 3: Summary of background estimates for the γ + $\geq$1 jet and γ + $\geq$2 jet data samples evaluated by Method B. Where two uncertainties are quoted, the first is statistical and the second is systematic.

Background	**γ + $\geq$1 Jet + $\not\!\!E_T$ > 20 GeV Sample**	**γ + $\geq$2 Jet + $\not\!\!E_T$ > 20 GeV Sample**
QCD (weighted)	127405 $\pm$ 357 $\pm$ 7040	40887 $\pm$ 202 $\pm$ 2103
Electroweak	6271 $\pm$ 79 $\pm$ 613	843 $\pm$ 29 $\pm$ 122
Diphoton	355 $\pm$ 19 $\pm$ 13	86 $\pm$ 9 $\pm$ 8
Non-Collision	124 $\pm$ 12 $\pm$ 4	8 $\pm$ 3 $\pm$ 1
γ + jets Data	134155 $\pm$ 366	41824 $\pm$ 204

Table 4: Summary of background estimates for the γ + $\geq$1 jet + $\not\!\!E_T$ > 20 GeV and γ + $\geq$2 jet + $\not\!\!E_T$ > 20 GeV data samples evaluated by Method B. Where two uncertainties are quoted, the first is statistical and the second is systematic.

Figures 2–5 show Method A results without the $\not\!\!E_T$ requirement, and Figures 6–9 show Method A results with the $\not\!\!E_T$ requirement. The data are represented by black circles, and the backgrounds are shown in different colors. As described in Section 3, the SM backgrounds include prompt γ production (labeled "γ MC"), QCD multi-jet production (labeled "QCD"), prompt diphoton production (labeled "Di-γ"), and electroweak production (labeled "EWK"). The non-collision backgrounds from cosmic rays and the beam halo are labeled "Non-collision." The top plot uses a logarithmic scale. The shaded region indicates the total systematic uncertainty, which includes the statistical uncertainty on the total background prediction.

The uncertainty due to the jet energy scale is by far the largest systematic uncertainty. Other sources of uncertainty that are taken into account include the following: parton density functions (PDFs), initial and final state radiation (ISR/FSR), dependence on the renormalization, factorization and normalization scales (Q^2), the strong coupling constant (α_s), the fake photon fraction determination, integrated luminosity, EM energy measurements, the beam halo estimate, and the cosmic ray background estimate.

We have measured the photon E_T spectrum from 30 GeV to about 550 GeV, and over this range the total systematic uncertainty increases from 15% to 90%. It is

evident that the photon purity increases at higher E_T. We are limited by statistics at high E_T. The invariant mass of the γ + leading jet extends up to 1000 GeV/c^2. Many background predictions become limited by statistics in the high mass region, and the systematic uncertainty increases from 15% to 90%. It is evident from these plots that the SM γ and QCD multijet backgrounds are dominant. However with the requirement of large $\not\!\!E_T$ in the event, these backgrounds are reduced and real $\not\!\!E_T$ from the electroweak processes (*e.g.* $W \to \ell\nu$) becomes significant. This $\not\!\!E_T$ requirement significantly improves the sensitivity to events in which a heavy particle is produced that we do not detect.

The backgrounds using Method A are well modeled and describe data reasonably well in most of the distributions. But a close inspection reveals discrepancies in certain distributions like lead jet E_T, H_T, jet multiplicity, and $\not\!\!E_T$, which are not within the systematic uncertainties. These kinematic distributions are most directly affected by the limitations of the leading-order predictions using PYTHIA.

Figures 10–13 show the Method B results without the $\not\!\!E_T$ requirement. The Figures 14–17 show the Method B results with the $\not\!\!E_T$ requirement. In these figures, "QCD (weighted)" indicates the weighted QCD background template that replaces the γ MC and QCD templates of Method A. Using Method B, we are able describe some distributions much better compared to Method A. The photon E_T distribution must agree with Method A by construction. The jet E_T, H_T, jet multiplicity and $\not\!\!E_T$ distributions, however, show significant improvement and agree well with data. The $\not\!\!E_T$ distribution agrees well in the low $\not\!\!E_T$ region. Some distributions using Method B were not modeled well as expected. For example the invariant mass of the photon and leading jet shows a large discrepancy, which is attributed to the fact that the QCD background events are from different processes (or Feynman diagrams).

5 Conclusions

We have presented results of the search for beyond SM physics in $\gamma + \geq$1 jet and $\gamma + \geq$2 jet events with and without a $\not\!\!E_T > 20$ GeV requirement. We have presented two different background prediction methods, Method A and Method B. Each method has proven to describe the γ + jets data with certain limitations. We conclude the two methods together provide a greater understanding of data than either method alone. Thus far, we see good agreement with Standard Model predictions extending over several orders of magnitude. The search for new heavy particles in the high $\not\!\!E_T$ events has shown no significant deviation from data. We conclude that all of our measurements are in agreement with the Standard Model expectation.

6 Acknowledgements

We thank the Fermilab staff and the technical staffs of the participating institutions for their vital contributions. This work was supported by the U.S. Department of Energy

and National Science Foundation; the Italian Istituto Nazionale di Fisica Nucleare; the Ministry of Education, Culture, Sports, Science and Technology of Japan; the Natural Sciences and Engineering Research Council of Canada; the National Science Council of the Republic of China; the Swiss National Science Foundation; the A.P. Sloan Foundation; the Bundesministerium für Bildung und Forschung, Germany; the World Class University Program, the National Research Foundation of Korea; the Science and Technology Facilities Council and the Royal Society, UK; the Institut National de Physique Nucleaire et Physique des Particules/CNRS; the Russian Foundation for Basic Research; the Ministerio de Ciencia e Innovación, and Programa Consolider-Ingenio 2010, Spain; the Slovak R&D Agency; and the Academy of Finland.

References

[1] F. Abe *et al.*, Nucl. Instrum. Methods Phys. Res. A **271**, 387 (1988); D. Amidei *et al.*, Nucl. Instum. Methods Phys. Res. A **350**, 73 (1994); F. Abe et al., Phys. Rev. D **52**, 4784 (1995); P. Azzi *et al.*, Nucl. Instrum. Methods Phys. Res. A **360**, 137 (1995); The CDF II Detector Technical Design Report, Fermilab-Pub-96/390-E.

[2] See for example S. Ambrosanio *et al.*, Phys. Rev. D **54**, 5395 (1996); or C.-H. Chen and J.F. Gunion, Phys. Rev. D **58**, 075005 (1998).

[3] S. Weinberg, "Implications of Dynamical Symmetry Breaking: An Addendum" Phys. Rev. **D19**, 1277–1280 (1979); L. Susskind, "Dynamics of Spontaneous Symmetry Breaking in the Weinberg-Salam Theory" Phys. Rev. **D20**, 2619–2625 (1979).

[4] F. Abe *et al.*, "Prompt photon cross section measurement in $\bar{p}p$ collisions at $\sqrt{s}$ = 1.8 TeV," Phys. Rev. D **48**, 2998–3025 (1993); F. Abe *et al.*, "Precision Measurement of the Prompt Photon Cross Section in $p\bar{p}$ Collisions at $\sqrt{s} = 1.8$ TeV," Phys. Rev. Lett. **73**, 2662 (1994).

[5] "The Timing System for the CDF Electromagnetic Calorimeters," Nucl. Instrum. Meth. A565:543–550, 2006.

[6] M. Goncharov *et al.*, "Discrimination of Beam Halo and Cosmic Rays as a Source of Photon Candidates," CDF-Note 8409.

[7] The CDF Collaboration, "Determination of the Jet Energy Scale at the Collider Detector at Fermilab," Nucl. Instrum. Meth. A566:375–412, 2006.

[8] T. Sjöstrand *et al.*, Comput. Phys. Commun. **135**, 238 (2001).

Figure 2: Kinematic distributions of $\gamma + \geq 1$ jet events using Method A. See Section 4 for a description of the elements in these distributions.

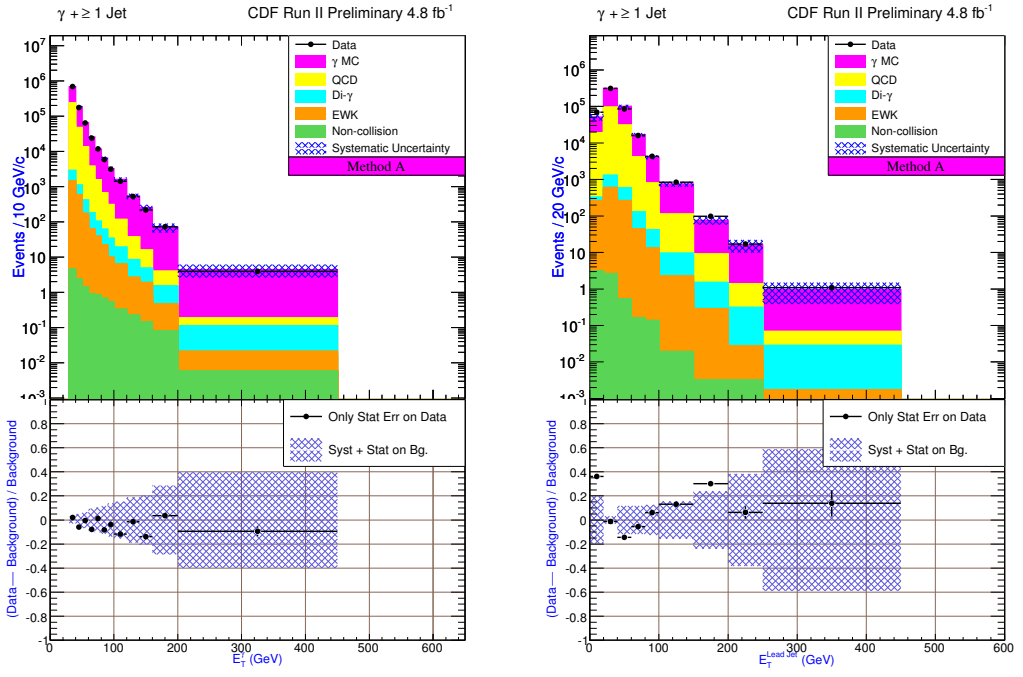

(a)

(b)

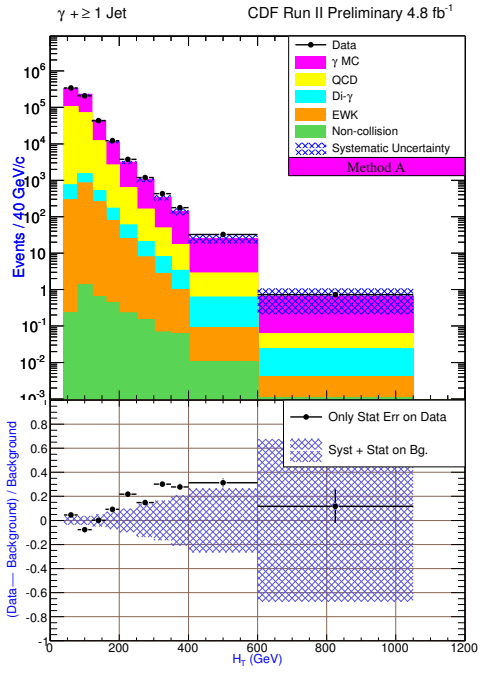

(c)

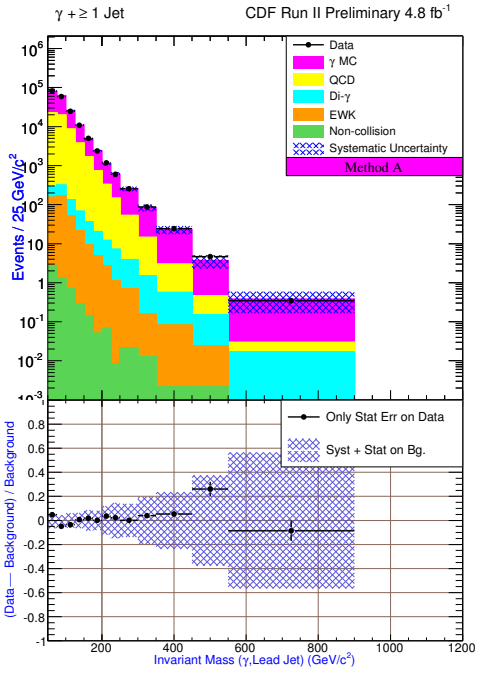

(d)

Figure 3: Kinematic distributions of $\gamma + \geq 1$ jet (top) and $\gamma + \geq 2$ jet (bottom) events using Method A. See Section 4 for a description of the elements in these distributions.

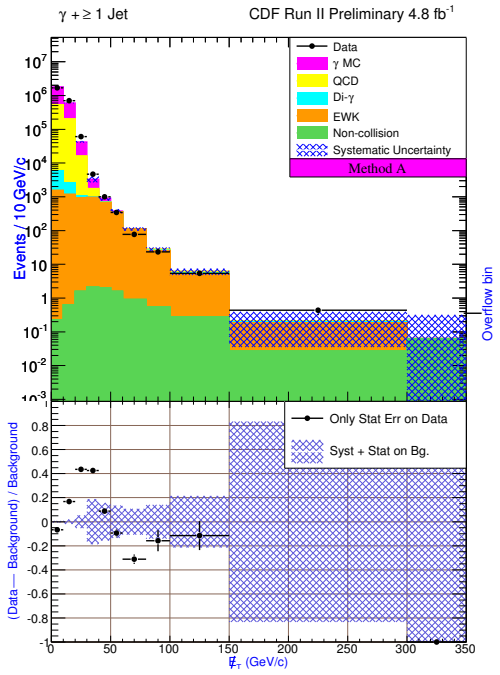

(a)

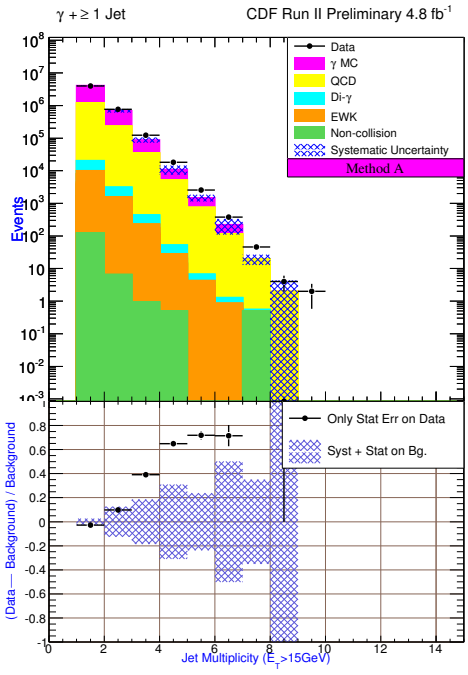

(b)

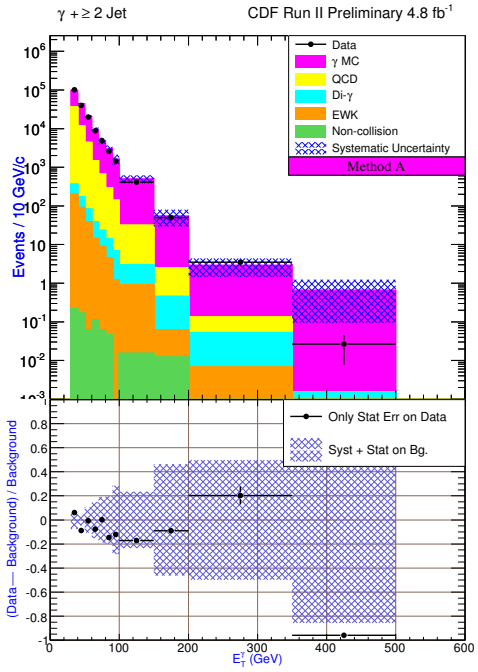

(c)

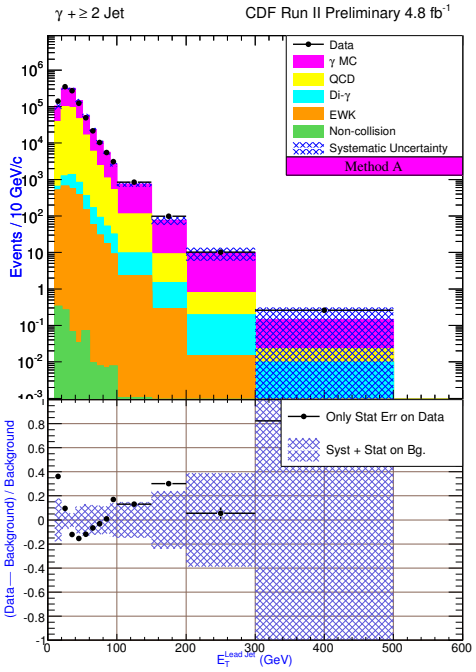

(d)

Figure 4: Kinematic distributions of $\gamma + \geq 2$ jet events using Method A. See Section 4 for a description of the elements in these distributions.

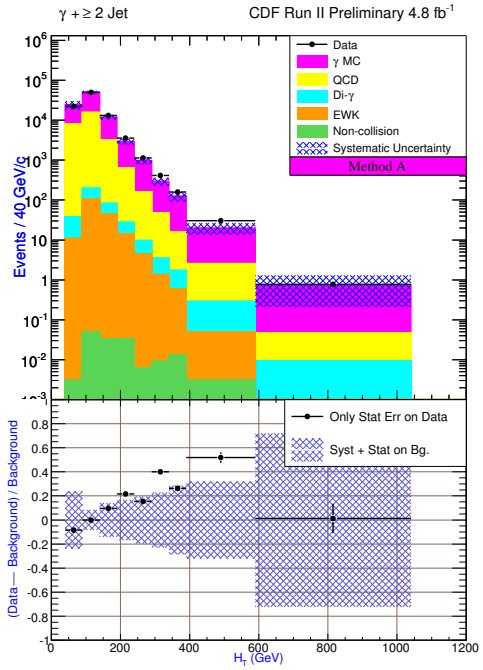

(a)

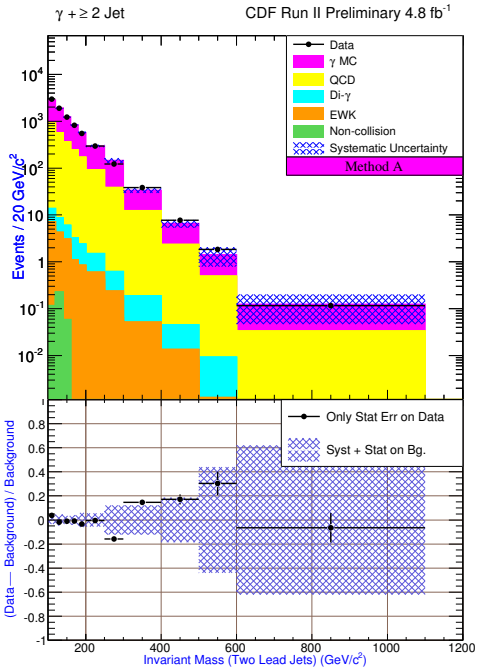

(b)

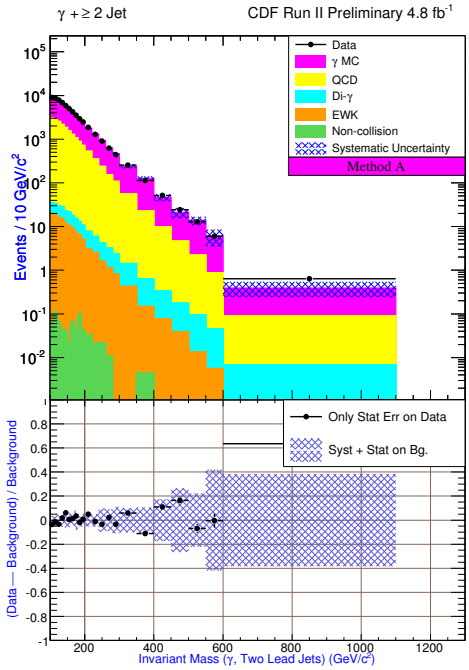

(c)

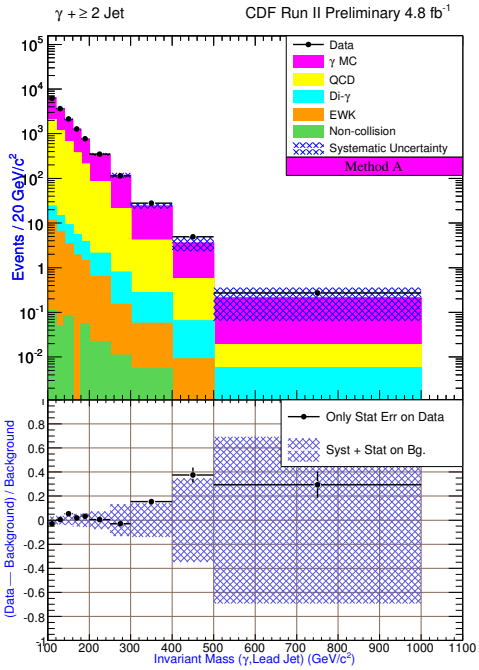

(d)

Figure 5: Kinematic distributions of γ + $\geq$2 jet events using Method A.

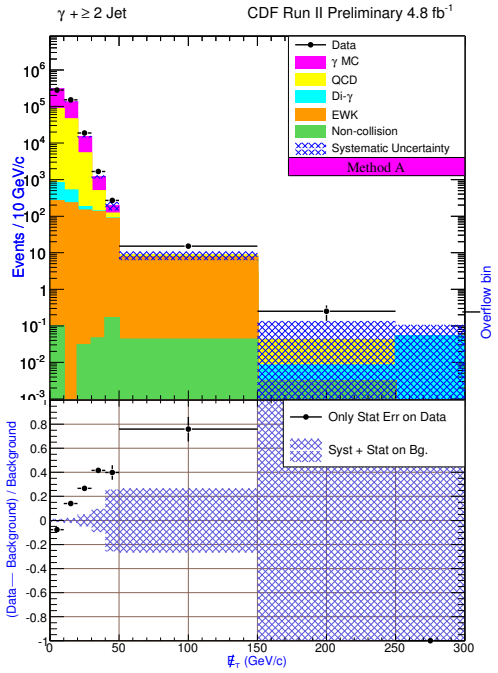

(a)

Figure 6: Kinematic distributions of $\gamma + \geq 1$ jet + $\not\!\!E_T > 20$ GeV events using Method A. See Section 4 for a description of the elements in these distributions.

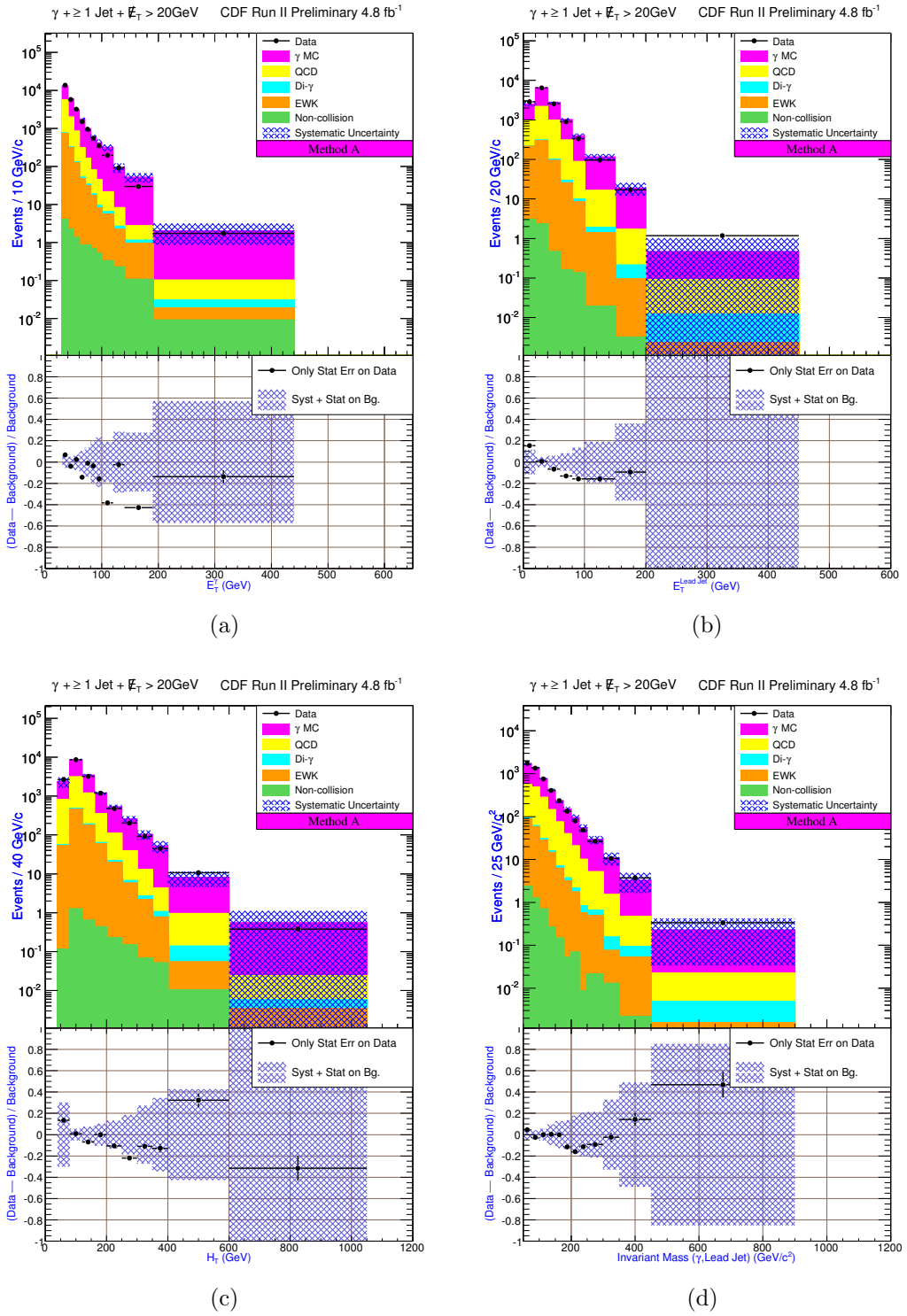

Figure 7: Kinematic distributions of $\gamma + \geq$1 jet + $\not\!\!E_T > 20$ GeV (top) and $\gamma + \geq$2 jet + $\not\!\!E_T > 20$ GeV (bottom) events using Method A. See Section 4 for a description of the elements in these distributions.

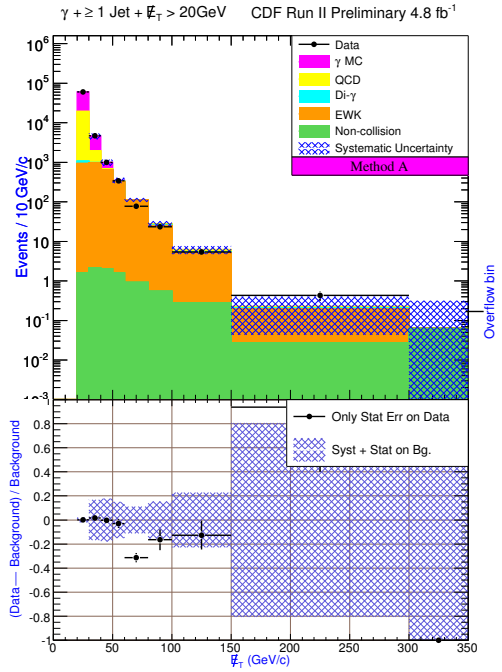

(a)

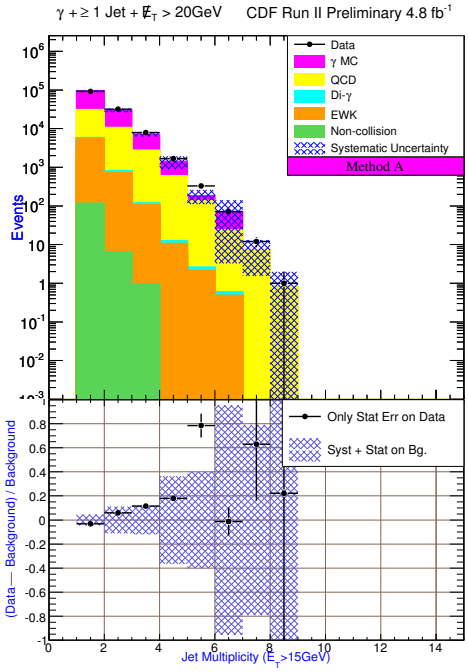

(b)

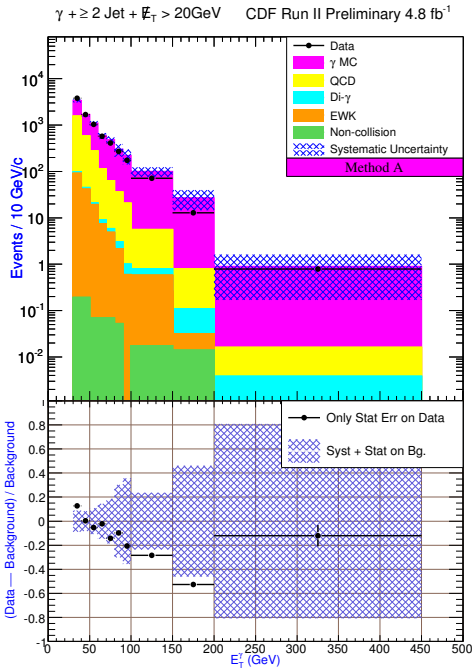

(c)

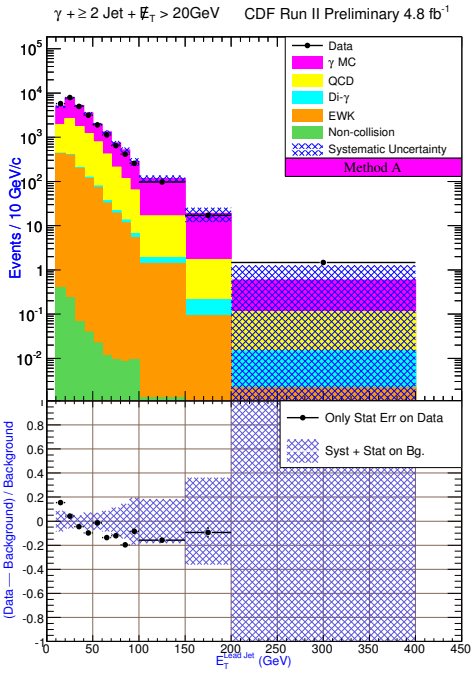

(d)

Figure 8: Kinematic distributions of $\gamma + \geq 2$ jet + $\not\!\!E_T > 20$ GeV events using Method A. See Section 4 for a description of the elements in these distributions.

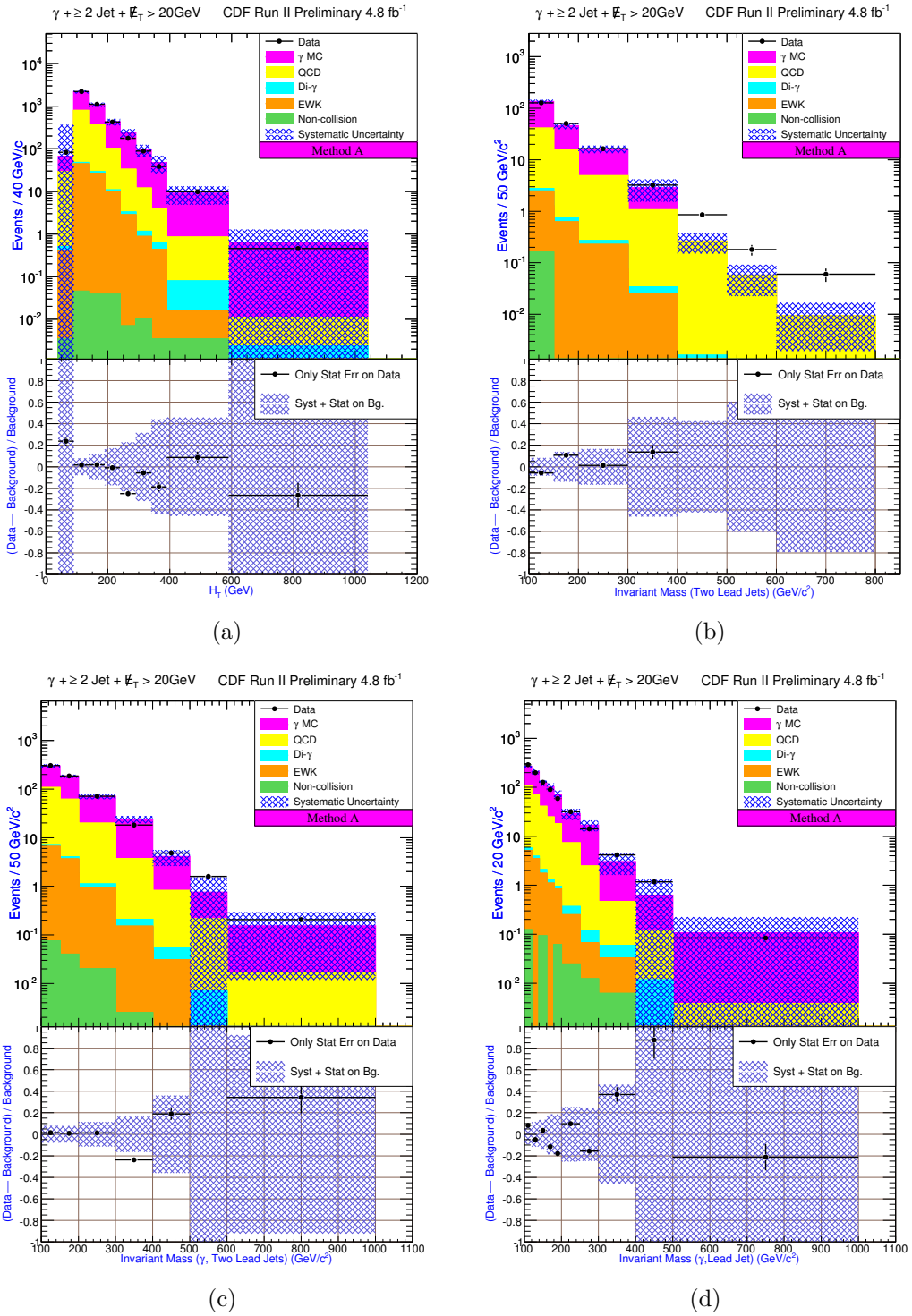

Figure 9: Kinematic distributions of $\gamma + \geq$2 jet + $\not\!\!E_T$ > 20 GeV events using Method A. See Section 4 for a description of the elements in these distributions.

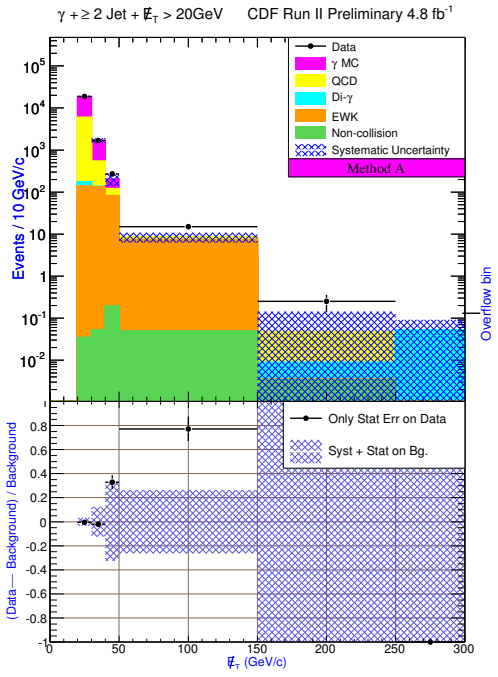

(a)

Figure 10: Kinematic distributions of $\gamma + \geq 1$ jet events using Method B. See Section 4 for a description of the elements in these distributions.

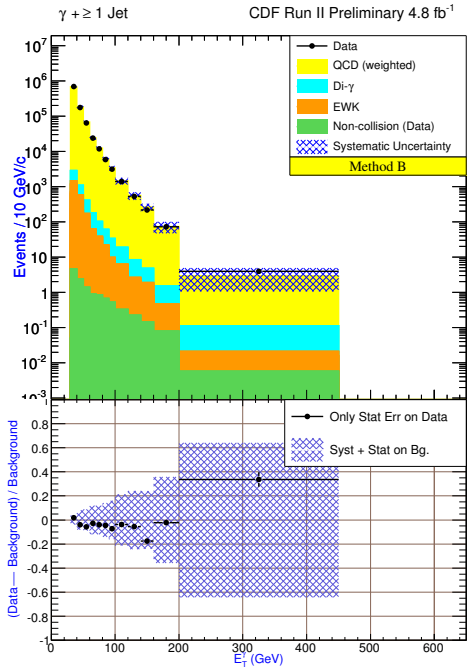

(a)

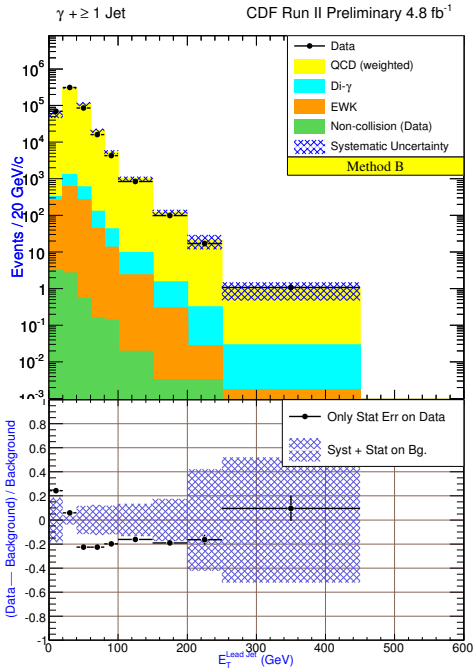

(b)

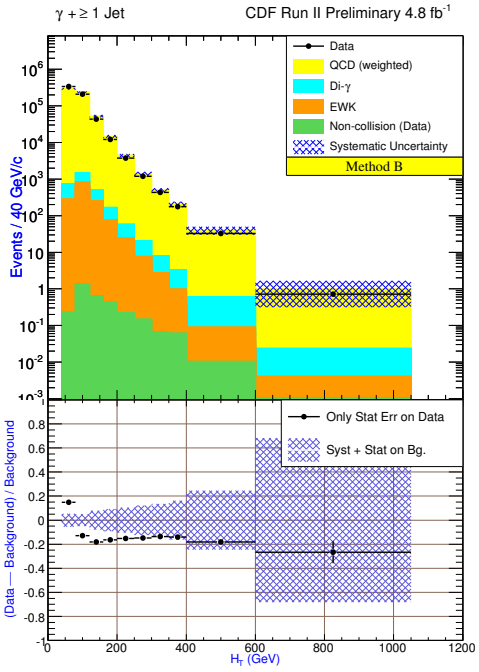

(c)

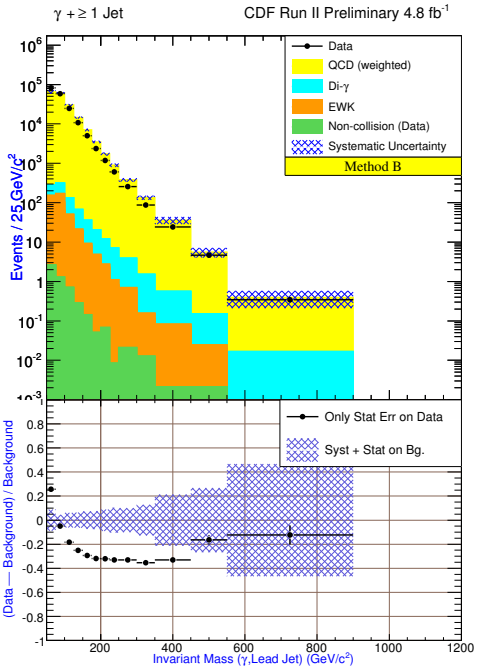

(d)

Figure 11: Kinematic distributions of $\gamma + \geq 1$ jet and $\gamma + \geq 2$ jet events using Method B. See Section 4 for a description of the elements in these distributions.

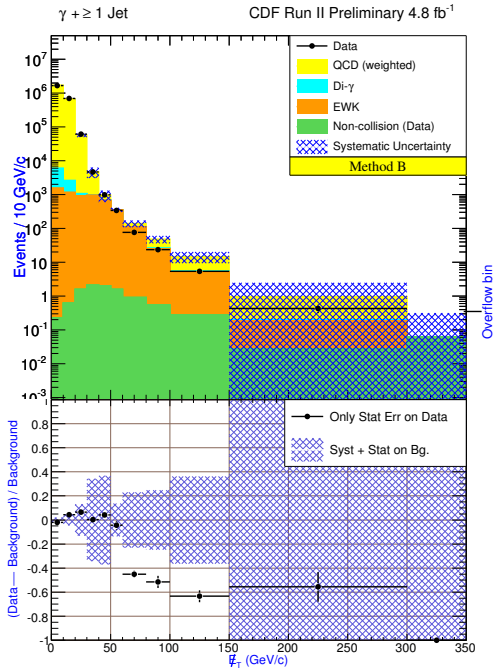

(a)

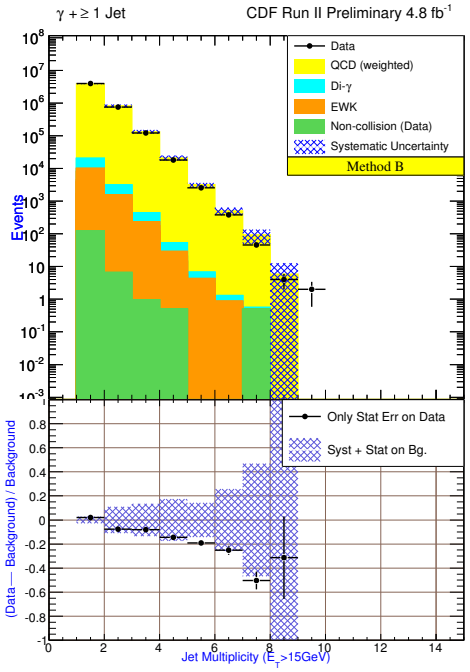

(b)

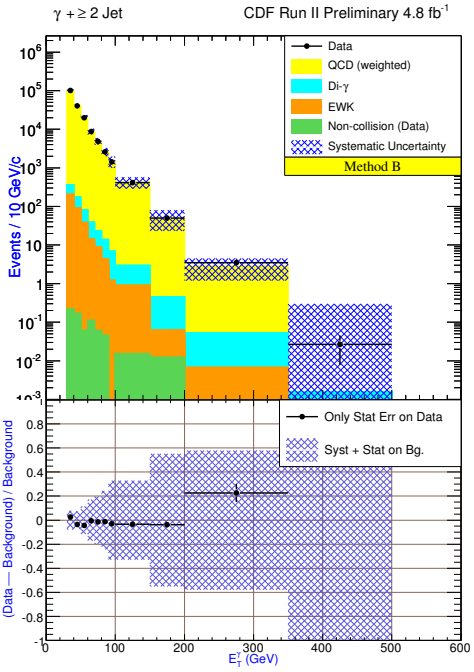

(c)

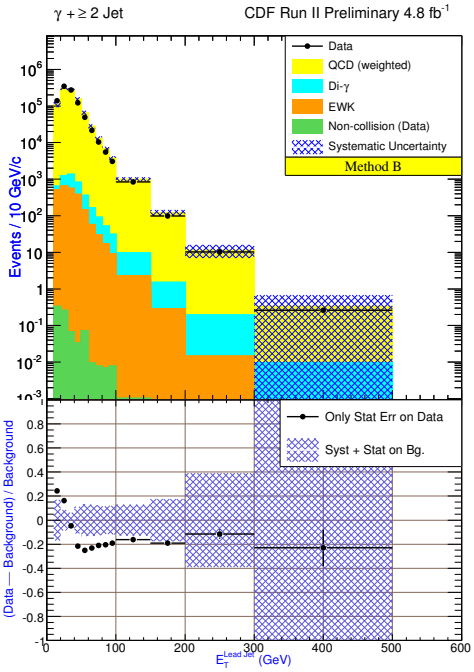

(d)

Figure 12: Kinematic distributions of $\gamma + \geq 2$ jet events using Method B. See Section 4 for a description of the elements in these distributions.

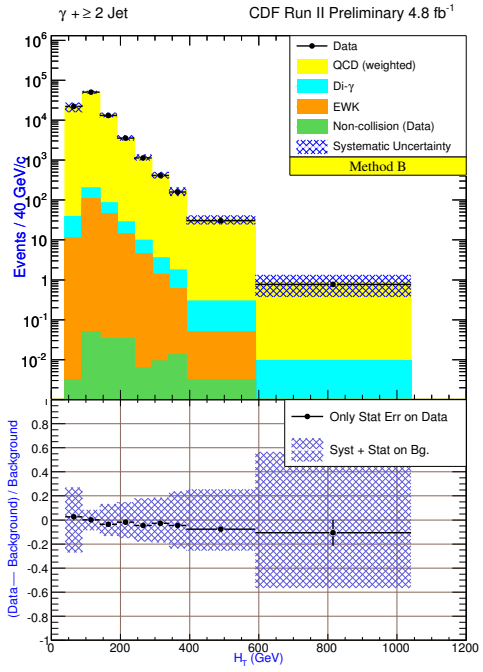

(a)

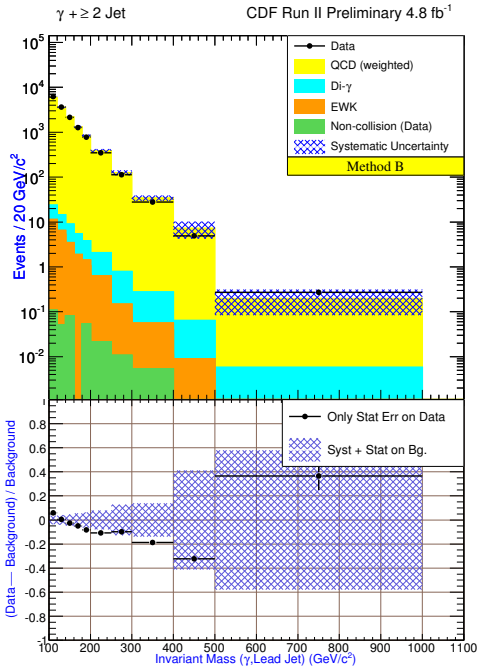

(b)

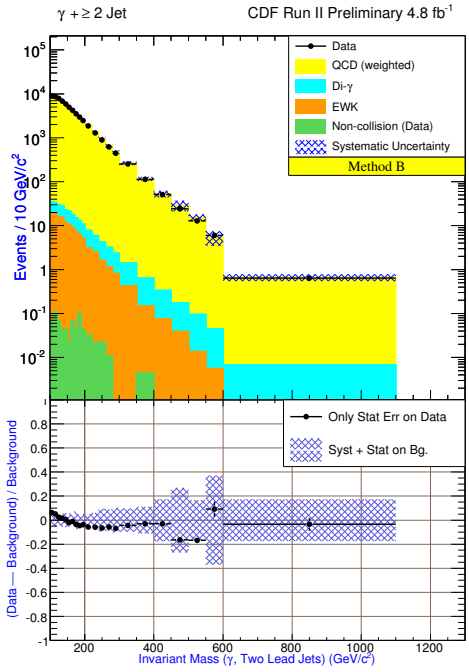

(c)

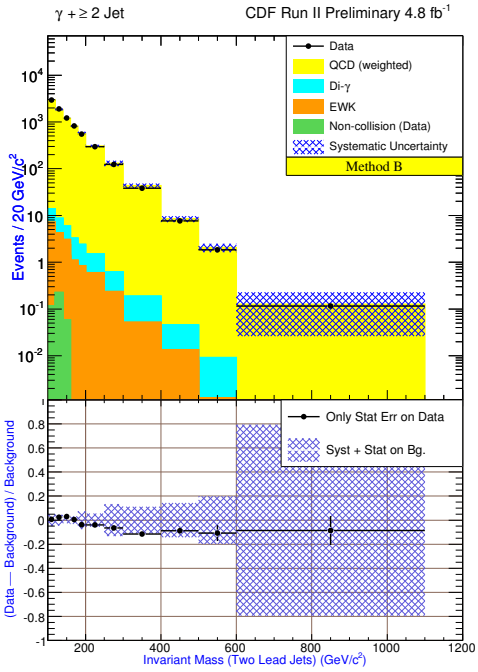

(d)

Figure 13: Kinematic distributions of $\gamma + \geq 2$ jet events using Method B. See Section 4 for a description of the elements in these distributions.

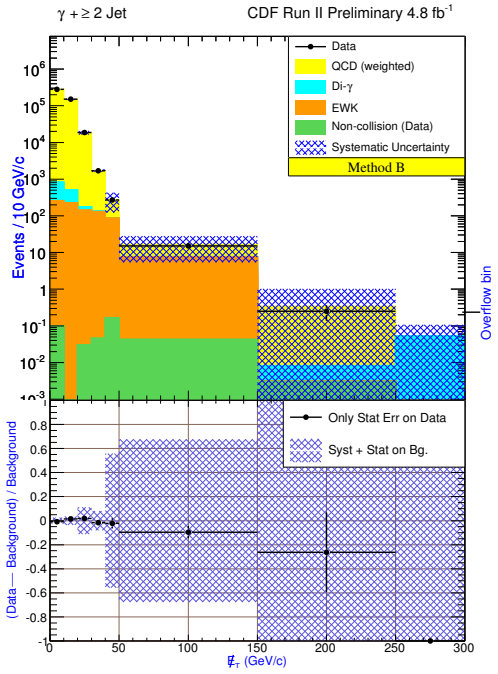

Figure 14: Kinematic distributions of $\gamma + \geq 1$ jet + $\not\!\!E_T > 20$ GeV events using Method B. See Section 4 for a description of the elements in these distributions.

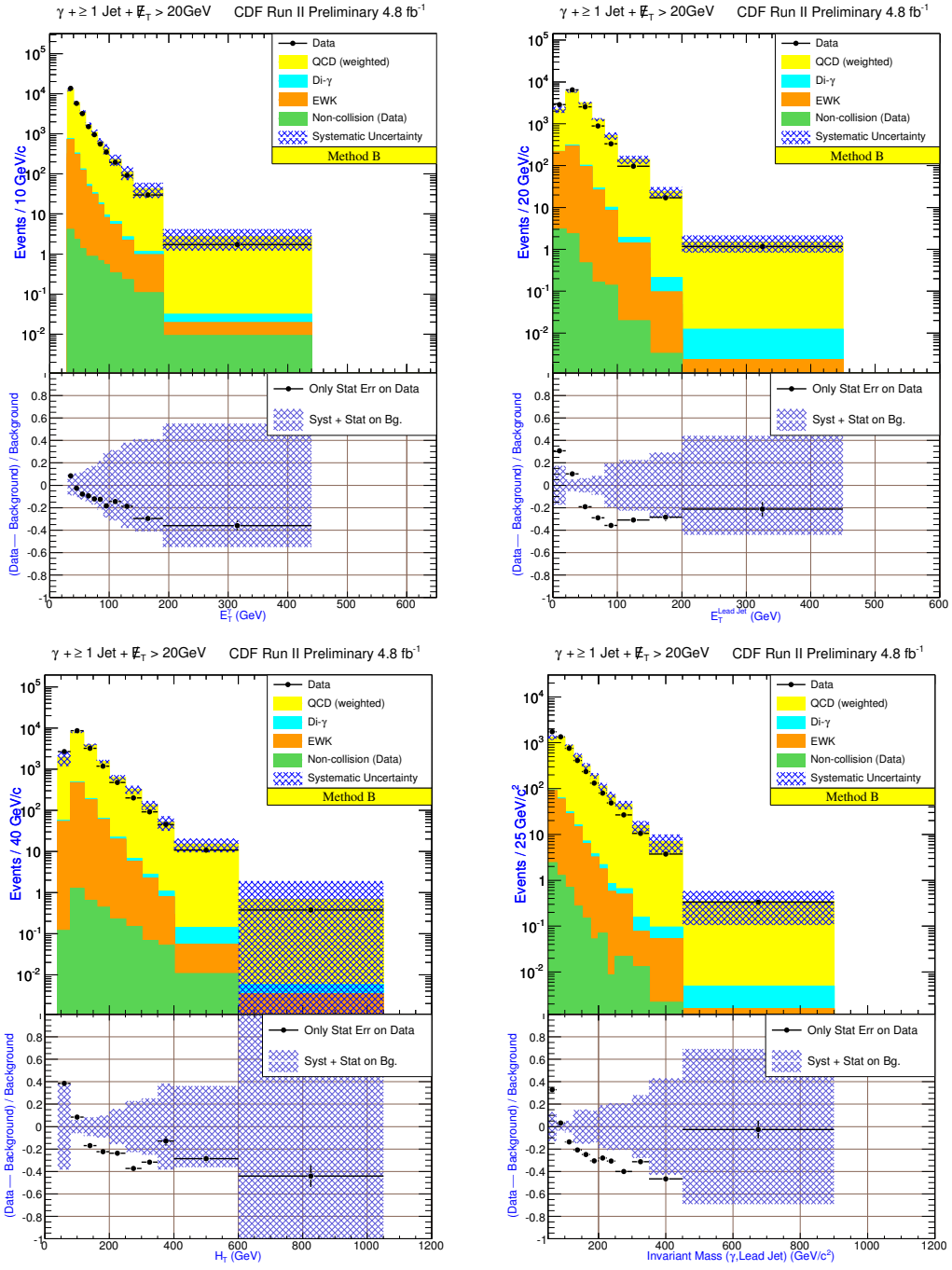

Figure 15: Kinematic distributions of $\gamma + \geq$1 jet + $\not\!\!E_T > 20$ GeV and $\gamma + \geq$2 jet + $\not\!\!E_T > 20$ GeV events using Method B. See Section 4 for a description of the elements in these distributions.

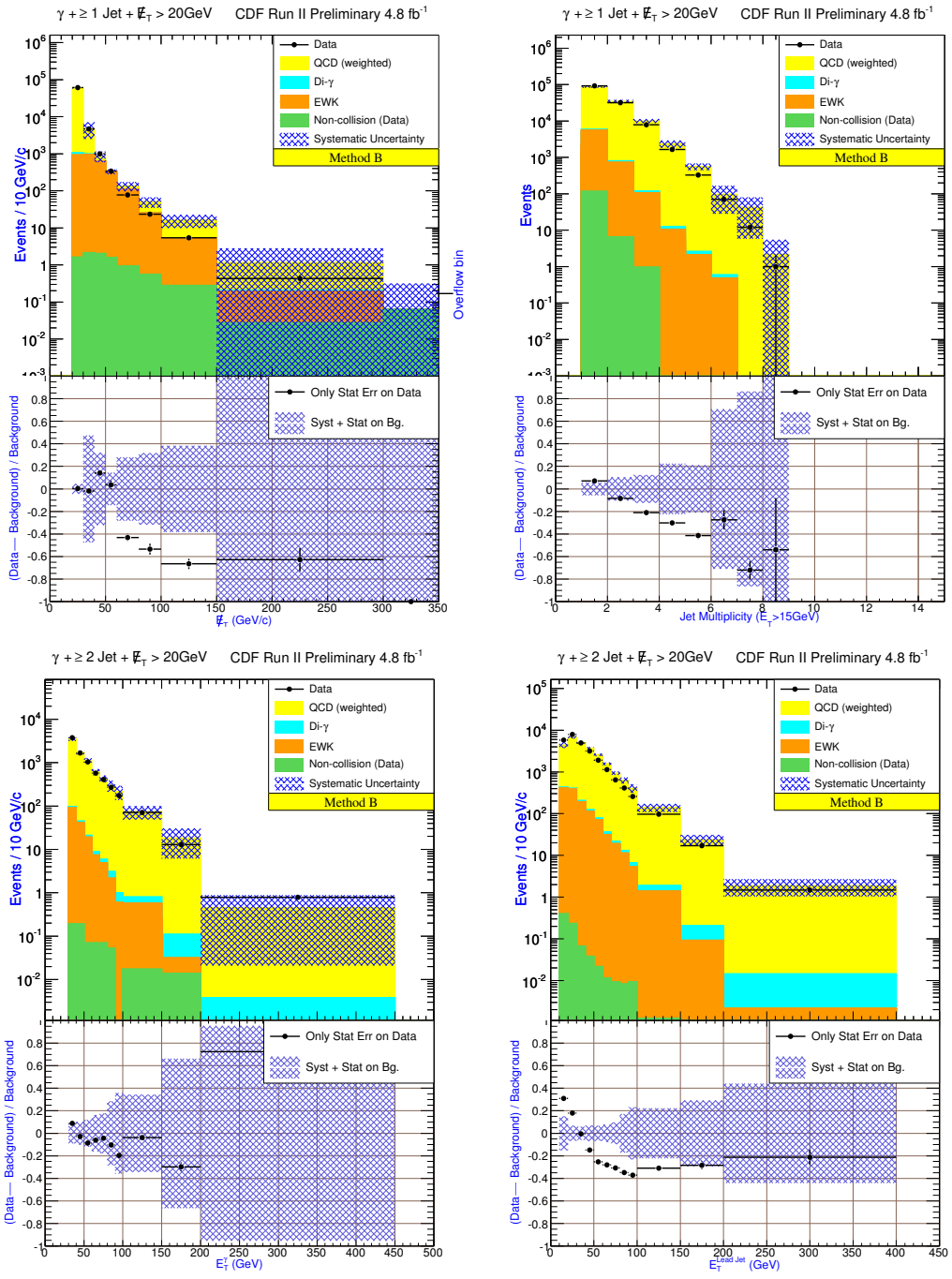

Figure 16: Kinematic distributions of $\gamma + \geq 2$ jet + $\not\!\!E_T > 20$ GeV events using Method B. See Section 4 for a description of the elements in these distributions.

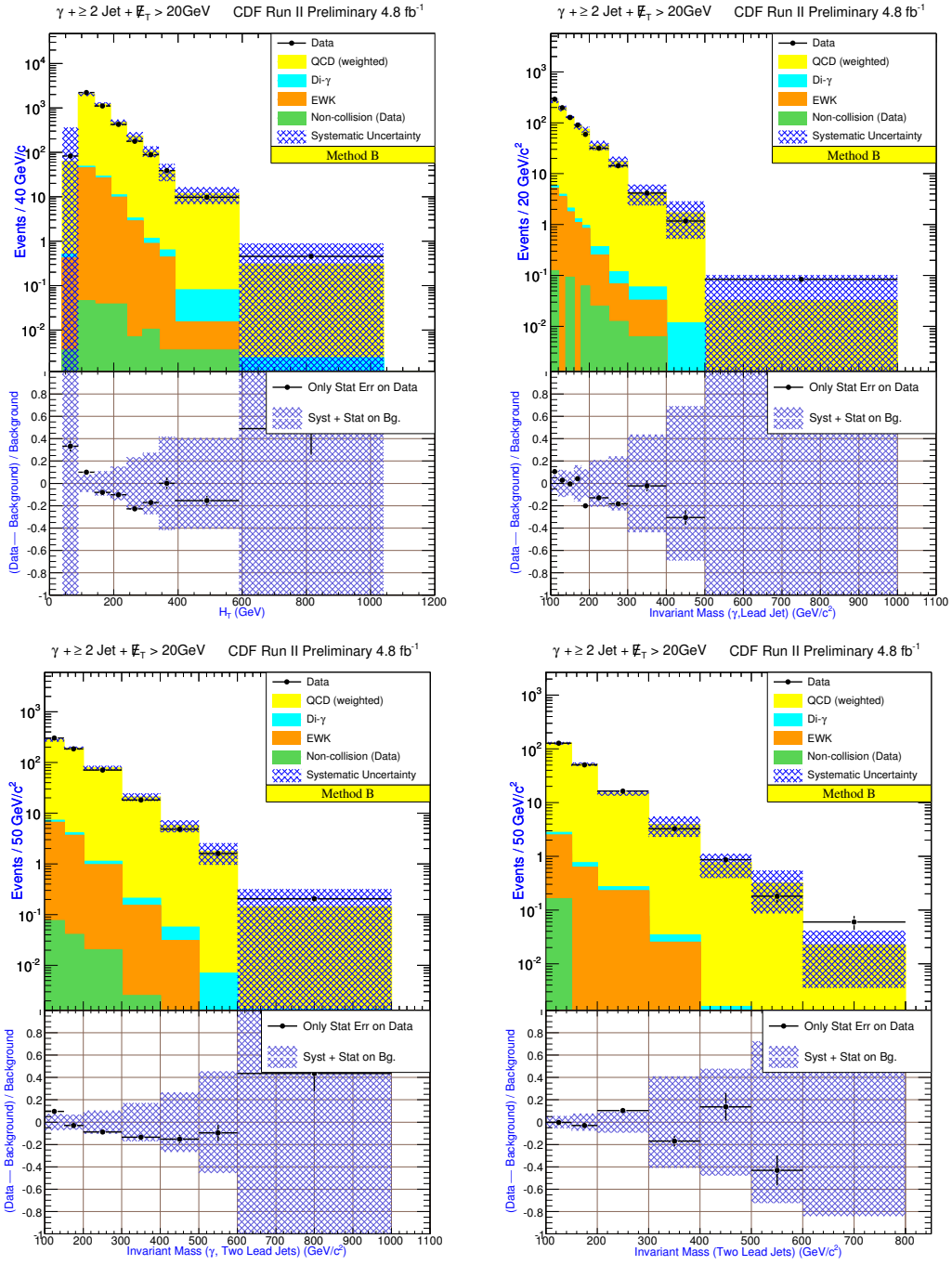

Figure 17: Kinematic distributions of $\gamma + \geq 2$ jet + $\not\!\!E_T > 20$ GeV events using Method B. See Section 4 for a description of the elements in these distributions.